Linear temporal and spatiotemporal stability analysis of two-layer falling films with density stratification

J. Hu,[1,*] X. Y. Yin,[2] H. Ben Hadid,[3] and D. Henry[3]
[1]*Institute of Applied Physics and Computational Mathematics, Beijing 100088, China*
[2]*Department of Modern Mechanics, University of Science and Technology of China, Hefei 230027, China*
[3]*Laboratoire de Mécanique des Fluides et d'Acoustique, CNRS/Université de Lyon, Ecole Centrale de Lyon/Université Lyon 1/INSA de Lyon, ECL, 36 avenue Guy de Collongue, 69134 Ecully Cedex, France*
(Received 19 June 2007; published 7 February 2008)

A detailed temporal and spatiotemporal stability analysis of two-layer falling films with density and viscosity stratification is performed by using the Chebyshev collocation method to solve the full system of linear stability equations. From the neutral curves Re(k) for the surface mode and the interface mode of instability, obtained for different density ratios γ of the upper layer to the lower layer, it is found that smaller density ratios make the surface mode and the short-wave interface mode much more stable, and can even make the short-wave interfacial instability disappear. Moreover, through the study of the local growth rates of the spatiotemporal instability as a function of the ray velocity V, it is found that for not too small incline angles like $\theta=0.2$, the two-layer flow is always convectively unstable, and there is a transition between long- and short-wave instabilities which is determined by the Briggs-Bers collision criterion. Due to the existence of the absolute Rayleigh-Taylor instability for $\gamma>0$ and $\theta=0$, a transition from convective to absolute instability can be detected at small incline angles, and the corresponding boundary curves are plotted for different Reynolds numbers, viscosity ratios, and incline angles. It is found that there exists a limit Reynolds number above which the two-layer film flow can only be convectively unstable for a fixed small incline angle. The spatial amplification properties of the convective waves are finally presented for both surface and interface modes.

DOI: 10.1103/PhysRevE.77.026302 PACS number(s): 47.15.gm

I. INTRODUCTION

The fluid dynamics of immiscible multiple-layered stratified shear flows is a fascinating and challenging subject in physics [1], which also has a practical interest for some environmental flows, such as rock glaciers [2], and for industrial processes, such as the coating of a color film which sometimes consists of more than ten different layers. It is thus important to explore the dynamical characteristics of multilayered liquid films. Kao [3,4] first investigated the long wave instability of the two-layer falling films for different heights, different densities, and different viscosities of the two layers. By using the same long-wave approximation as Yih [5] for one-layer films, he obtained two critical Reynolds numbers corresponding to two different modes of instability, now usually regarded as the surface mode and the interface mode. When the less viscous layer is adjacent to the plate, the interfacial instability occurs below a critical Reynolds number and thus exists even when the Reynolds number approaches zero, i.e., in inertialess conditions. Later, Loewenherz and Lawrence [2] studied the inertialess instabilities through a zero-Reynolds-number approximation to the Orr-Sommerfeld equations. They focused on the role of the viscosity stratification, assuming equal density in the two layers. They showed that the inertialess interfacial instability can occur at finite wavelength. Later, in a detailed study which still assumes equal-density layers, Chen [6] verified that the unstable wave motion, generated when the less viscous layer is in the region next to the wall, can occur for any Reynolds number and any finite interface and surface tension. Recently, Hu *et al.* [7] pointed out that there exists a critical density ratio below which the finite-wavelength inertialess interfacial instability disappears. By use of a kinetic energy budget, Jiang *et al.* [8] also revealed that the work done by the shear stress at the unperturbed free surface is essential to cause the inertialess interfacial instability.

Linear stability analyses of falling films with more than two layers have also been performed. Akhtaruzzaman *et al.* [9] first investigated the long-wavelength motion of a three-layer system. Then Wang *et al.* [10] adopted the long-wave asymptotic method of Yih [5] and identified the long-wave instability of the three-layer system. They also studied a five-layered film flow and showed that a downward step decrease in viscosity across an interface makes the five-layered system unstable for any small Reynolds number. For a three-layer system, Weinstein and Kurz [11] furthermore identified an inertialess long-wave instability when the middle-layer viscosity or density is smaller than those of the adjacent layers. Weinstein and Chen [12] later studied large growth rate instabilities in three-layer flows at zero Reynolds number. They found that the long-wavelength inertialess interfacial instability of Weinstein and Kurz [11] persists in the finite-wavelength domain in the form of a pair of waves with nearly complex conjugate wave speeds. These linear instability analyses for multiple layers all showed that the number of unstable modes is generally equal to the number of interfaces (including the free surface) in the problem.

The spatiotemporal instability analyses of these multilayer film flows are, in contrast, very few. For a single-layer falling film, the absolute and convective instability has been thoroughly studied by Brevdo *et al.* [13]. They used the full

*hu_jun@iapcm.ac.cn

linearized Navier-Stokes equations to investigate the characteristics of the absolute or convective instability through the exact Briggs-Bers collision criterion. They explored a large region of the parameter space and pointed out that the one-layer film flow is convectively unstable, which agrees with all performed experiments. They further studied the properties of spatially amplifying waves and found results in complete agreement with the experiments performed by Liu *et al.* [14,15]. Recently Hu *et al.* [7] performed the first spatiotemporal study in a multilayer film flow. They investigated the absolute and convective properties of the interfacial instability of the two-layer film flow by using the Briggs-Bers collision criterion. Under the zero-Reynolds-number and zero-surface-tension approximation, the transition from convective (CI) to absolute instability (AI) has been detected at small incline angle. Furthermore, the AI/CI boundary curves show that smaller viscous ratios make the two-layer film flow absolutely unstable at smaller density ratios, and that the minimum critical density ratio occurs at moderate depth ratio. In the large region of the parameter space where the two-layer film flow is convectively unstable, both long and short waves with different downstream velocities have been detected.

In this paper, we study the effect of inertia on the temporal and spatiotemporal instabilities of the two-layer film flow. The full system of linear stability equations is solved by a Chebyshev collocation method (Sec. II). The results of the linear temporal approach are presented in Sec. III: the effects of inertia and density stratification on the onset of both interface and surface modes are characterized for two situations with different depth and viscous ratios. We then study the spatiotemporal nature (absolute or convective) of the instability of the two-layer film flow. The properties of the convective instabilities that prevail in the two-layer film flow are first determined (Sec. IV). A transition from convective to absolute instability is, however, detected for small inclinations of the plate, and the corresponding boundary curves are calculated for increasing inertia and for various depth, density, and viscosity ratios (Sec. V). Finally, Sec. VI is devoted to the study of the properties of the spatially amplifying waves in the region of parameters where the instability is convective.

II. FORMULATION

We consider a two-dimensional gravity-driven laminar flow of two liquid layers down an inclined flat plate tilted at an angle θ to the horizontal (Fig. 1). The two layers have different thicknesses d_i, densities ρ_i, and dynamical viscosities μ_i (the subscript $i=1,2$ denotes the lower and upper fluids, respectively).

For undisturbed two-layer falling films, the integral average streamwise velocity u_a driven by the $g \sin\theta$ component of gravity along the plate can be derived as

$$u_a = \frac{\rho_1 g \sin\theta\, d_1^2}{K\mu_1}, \tag{1}$$

where

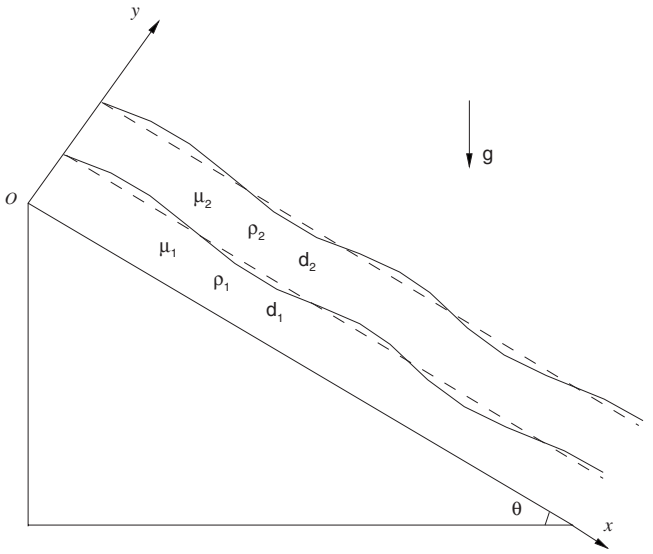

FIG. 1. Schematic representation of the two-layer falling films.

$$K = \left(\frac{1+\delta}{\gamma\left(\frac{\delta}{2} + \delta^2 + \frac{\delta^3}{3m}\right) + \left(\frac{1}{3} + \frac{\delta}{2}\right)} \right),$$

and

$$\delta = \frac{d_2}{d_1}, \quad \gamma = \frac{\rho_2}{\rho_1}, \quad m = \frac{\mu_2}{\mu_1}$$

represent the ratios of depths, densities, and dynamical viscosities, respectively (upper layer to lower layer).

The dimensionless governing equations are

$$\frac{\partial u_i}{\partial x} + \frac{\partial v_i}{\partial y} = 0, \tag{2a}$$

$$\frac{\partial u_i}{\partial t} + u_i\frac{\partial u_i}{\partial x} + v_i\frac{\partial u_i}{\partial y} = -\frac{\partial p_i}{\partial x} + \frac{\sin\theta}{\mathrm{Fr}^2} + \frac{1}{R_i}\Delta u_i, \tag{2b}$$

$$\frac{\partial v_i}{\partial t} + u_i\frac{\partial v_i}{\partial x} + v_i\frac{\partial v_i}{\partial y} = -\frac{\partial p_i}{\partial y} - \frac{\cos\theta}{\mathrm{Fr}^2} + \frac{1}{R_i}\Delta v_i, \tag{2c}$$

where $i=1,2$ and $\Delta = \partial^2/\partial x^2 + \partial^2/\partial y^2$. Here the pressures $\tilde{p}_i$ in the two layers are nondimensionalized as $p_i = (\tilde{p}_i - \tilde{p}_0)/\rho_i u_a^2$. The characteristic length is the height of the lower layer d_1 and the characteristic velocity is the average velocity u_a. The Reynolds numbers and the Froude number which are involved in the equations are defined as

$$\mathrm{Re} = R_1 = \frac{\rho_1 u_a d_1}{\mu_1}, \quad R_2 = \frac{\gamma}{m}R_1 = \frac{\rho_2 u_a d_1}{\mu_2}, \quad \mathrm{Fr} = \frac{u_a}{(g d_1)^{1/2}}, \tag{3}$$

so that $K\,\mathrm{Fr}^2 = R_1 \sin\theta$. Thus, only one Reynolds number is needed, which we choose to be Re. The basic dimensionless streamwise velocity U_1, U_2 and pressure P_1, P_2 solutions of the system (2a)–(2c) are given by

$$U_1(y) = K\left(-\frac{y^2}{2} + (1+\gamma\delta)y\right), \quad 0 \le y \le 1, \tag{4a}$$

$$U_2(y) = K\left(-\frac{\gamma}{2m}y^2 + \frac{(1+\delta)\gamma}{m}y + \frac{1}{2} - \frac{\gamma}{2m} + \gamma\delta - \frac{\gamma\delta}{m}\right), \quad 1 \le y \le 1+\delta, \tag{4b}$$

$$P_1(y) = \frac{\cos\theta}{\mathrm{Fr}^2}(1+\gamma\delta - y), \quad 0 \le y \le 1, \tag{4c}$$

$$P_2(y) = \frac{\cos\theta}{\mathrm{Fr}^2}(1+\delta - y), \quad 1 \le y \le 1+\delta. \tag{4d}$$

Due to the different nondimensionalization of the pressure in the two layers, the equality of the pressures at the interface yields $P_1 = \gamma P_2$ at $y=1$.

In the general case of a perturbed two-layer system (Fig. 1), for which ξ and η are the dimensionless deviations from the undisturbed free surface and interface positions, respectively, the dimensionless boundary conditions corresponding to no-slip and no-penetration boundary conditions along both the inclined wall and the interface, and to one kinematic and two dynamical boundary conditions along both the interface and the free surface, are given by

$$u_1 = v_1 = 0 \quad \text{at } y = 0, \tag{5a}$$

$$u_1 = u_2, \quad v_1 = v_2 \quad \text{at } y = 1 + \eta(x,t), \tag{5b}$$

$$\frac{\partial \eta}{\partial t} + u_1\frac{\partial \eta}{\partial x} = v_1 \quad \text{at } y = 1 + \eta(x,t), \tag{5c}$$

$$(1-\eta_x^2)\left(\frac{\partial u_1}{\partial y} + \frac{\partial v_1}{\partial x}\right) + 4\eta_x\frac{\partial v_1}{\partial y} = m(1-\eta_x^2)\left(\frac{\partial u_2}{\partial y} + \frac{\partial v_2}{\partial x}\right) + 4m\eta_x\frac{\partial v_2}{\partial y} \quad \text{at } y = 1 + \eta(x,t), \tag{5d}$$

$$p_1(1+\eta_x^2) + \frac{2}{R_1}\left[(1-\eta_x^2)\frac{\partial u_1}{\partial x} + \eta_x\left(\frac{\partial u_1}{\partial y} + \frac{\partial v_1}{\partial x}\right)\right] + 2H_{c1}S_1(1+\eta_x^2) = \gamma p_2(1+\eta_x^2) + \frac{2\gamma}{R_2}\left[(1-\eta_x^2)\frac{\partial u_2}{\partial x} + \eta_x\left(\frac{\partial u_2}{\partial y} + \frac{\partial v_2}{\partial x}\right)\right] \quad \text{at } y = 1 + \eta(x,t), \tag{5e}$$

$$\frac{\partial \xi}{\partial t} + u_2\frac{\partial \xi}{\partial x} = v_2 \quad \text{at } y = 1 + \delta + \xi(x,t), \tag{5f}$$

$$(1-\xi_x^2)\left(\frac{\partial u_2}{\partial y} + \frac{\partial v_2}{\partial x}\right) + 4\xi_x\frac{\partial v_2}{\partial y} = 0 \quad \text{at } y = 1 + \delta + \xi(x,t), \tag{5g}$$

$$\gamma p_2(1+\xi_x^2) + \frac{2\gamma}{R_2}\left[(1-\xi_x^2)\frac{\partial u_2}{\partial x} + \xi_x\left(\frac{\partial u_2}{\partial y} + \frac{\partial v_2}{\partial x}\right)\right] + 2H_{c2}S_2(1+\xi_x^2) = 0 \quad \text{at } y = 1 + \delta + \xi(x,t), \tag{5h}$$

where

$$2H_{c1} = \frac{\eta_{xx}}{(1+\eta_x^2)^{3/2}}, \quad S_1 = \frac{\sigma_1}{\rho_1 u_a^2 d_1},$$

$$2H_{c2} = \frac{\xi_{xx}}{(1+\xi_x^2)^{3/2}}, \quad S_2 = \frac{\sigma_2}{\rho_1 u_a^2 d_1}.$$

The disturbed flow can be decomposed into $u_i = U_i + u_i'$, $v_i = v_i'$, and $p_i = P_i + p_i'$, and the deviations ξ and η can be considered to be of the same order as the above perturbation quantities. We can thus derive the linearized governing equations,

$$\frac{\partial u_i'}{\partial x} + \frac{\partial v_i'}{\partial y} = 0, \tag{6a}$$

$$\frac{\partial u_i'}{\partial t} + U_i\frac{\partial u_i'}{\partial x} + \frac{dU_i}{dy}v_i' = -\frac{\partial p_i'}{\partial x} + \frac{1}{R_i}\Delta u_i', \tag{6b}$$

$$\frac{\partial v_i'}{\partial t} + U_i\frac{\partial v_i'}{\partial x} = -\frac{\partial p_i'}{\partial y} + \frac{1}{R_i}\Delta v_i', \tag{6c}$$

where $i=1,2$, and the linearized boundary conditions,

$$u_1' = v_1' = 0 \quad \text{at } y = 0, \tag{7a}$$

$$u_1' + \frac{dU_1}{dy}\eta = u_2' + \frac{dU_2}{dy}\eta, \quad v_1' = v_2' \quad \text{at } y = 1, \tag{7b}$$

$$\frac{\partial \eta}{\partial t} + U_1\frac{\partial \eta}{\partial x} = v_1' \quad \text{at } y = 1, \tag{7c}$$

$$\left(\frac{\partial u_1'}{\partial y} + \frac{\partial v_1'}{\partial x} + \frac{d^2U_1}{dy^2}\eta\right) = m\left(\frac{\partial u_2'}{\partial y} + \frac{\partial v_2'}{\partial x} + \frac{d^2U_2}{dy^2}\eta\right) \quad \text{at } y = 1, \tag{7d}$$

$$p_1' + \frac{dP_1}{dy}\eta + \frac{2}{R_1}\frac{\partial u_1'}{\partial x} + S_1\eta_{xx} = \gamma p_2' + \gamma\frac{dP_2}{dy}\eta + \frac{2\gamma}{R_2}\frac{\partial u_2'}{\partial x} \quad \text{at } y = 1, \tag{7e}$$

$$\frac{\partial \xi}{\partial t} + U_2\frac{\partial \xi}{\partial x} = v_2' \quad \text{at } y = 1 + \delta, \tag{7f}$$

$$\frac{\partial u_2'}{\partial y} + \frac{\partial v_2'}{\partial x} + \frac{d^2U_2}{dy^2}\xi = 0 \quad \text{at } y = 1 + \delta, \tag{7g}$$

$$\gamma p_2' + \gamma\frac{dP_2}{dy}\xi + \frac{2\gamma}{R_2}\frac{\partial u_2'}{\partial x} + S_2\xi_{xx} = 0 \quad \text{at } y = 1 + \delta. \tag{7h}$$

Now we assume that there are normal mode solutions of the form

$$u_i'(y,x,t) = \hat{u}_i(y)e^{i(kx-\omega t)}, \quad v_i'(y,x,t) = \hat{v}_i(y)e^{i(kx-\omega t)},$$

$$p_i'(y,x,t) = \hat{p}_i(y)e^{i(kx-\omega t)}, \quad \xi = \hat{\xi}e^{i(kx-\omega t)}, \quad \eta = \hat{\eta}e^{i(kx-\omega t)}. \tag{8}$$

Substituting them into the disturbed linearized governing equations and the corresponding boundary conditions, then eliminating the disturbed pressure p' and disturbed streamwise velocity u', yields the linear stability equations (Orr-Sommerfeld equations) for the two fluids,

$$(D^2-k^2)^2\hat{v}_i = iR_i[(U_ik-\omega)(D^2-k^2) - D^2U_ik]\hat{v}_i, \tag{9}$$

where $D=d/dy$.

The linear boundary conditions at the plate wall, the interface, and the free surface become

$$\hat{v}_1 = D\hat{v}_1 = 0 \quad \text{at } y=0, \tag{10a}$$

$$D\hat{v}_1 - D\hat{v}_2 = ik(DU_1 - DU_2)\hat{\eta}, \quad \hat{v}_1 = \hat{v}_2 \quad \text{at } y=1, \tag{10b}$$

$$i(U_1k-\omega)\hat{\eta} = \hat{v}_1 \quad \text{at } y=1, \tag{10c}$$

$$(D^2+k^2)\hat{v}_1 - iD^2U_1k\hat{\eta} = m[(D^2+k^2)\hat{v}_2 - iD^2U_2k\hat{\eta}] \quad \text{at } y=1, \tag{10d}$$

$$m[D^2-3k^2-iR_2(U_2k-\omega)]D\hat{v}_2 - [D^2-3k^2 - iR_1(U_1k-\omega)]D\hat{v}_1 + i(\gamma DU_2 - DU_1)R_1k\hat{v}_2 - [(\gamma-1)K\cot\theta - R_1S_1k^2]k^2\hat{\eta} = 0 \quad \text{at } y=1, \tag{10e}$$

$$i(U_2k-\omega)\hat{\xi} = \hat{v}_2 \quad \text{at } y=1+\delta, \tag{10f}$$

$$(D^2+k^2)\hat{v}_2 - iD^2U_2k\hat{\xi} = 0 \quad \text{at } y=1+\delta, \tag{10g}$$

$$m[D^2-3k^2-iR_2(U_2k-\omega)]D\hat{v}_2 - (\gamma K\cot\theta + R_1S_2k^2)k^2\hat{\xi} = 0 \quad \text{at } y=1+\delta. \tag{10h}$$

The two Orr-Sommerfeld (OS) equations are ordinary differential equations in terms of $\hat{v}_i$ and can be regarded as a two-point boundary value problem. If there exists a nontrivial solution for the equations, a corresponding dispersion relation $D(k,\omega;\mathrm{Re},\delta,\gamma,m,S_1,S_2,\theta)=0$ should be satisfied, and an eigenvalue problem has to be solved. Because it is impossible to find the explicit analytical dispersion relation if there is no further simplification such as long-wave approximation or zero-Reynolds-number approximation, the dispersion relation has to be obtained numerically. In this paper, similarly to the method of Chen [6] to study the situation $\gamma=1$, i.e., without density stratification, the Chebyshev collocation method [16] is used to discretize the equations, and the QZ algorithm is utilized to solve the resulting general eigenvalue problem. A mapping technique proposed by Goussis and Pearlstein [17] is used in our code to map the infinite spurious eigenvalues to a specified point in the complex plane.

III. TEMPORAL INSTABILITY

The long-wave instability analysis of Kao [3,4] has already revealed that the two-layer film flow can be destabilized by two different modes, a surface mode and an interface mode. The surface mode is similar to that observed in the one-layer film flow, and it is triggered above a critical Reynolds number. The interface mode, on the contrary, is triggered below a critical Reynolds number when the less viscous layer is adjacent to the plate. This indicates that the interface mode corresponds to an inertialess instability. These two modes have already been studied in detail by Loewenherz and Lawrence [2] and Chen [6] for equal-density layers ($\gamma=1$). The main applications, however, are concerned with layers of different densities. We thus choose to focus our study in this section on the influence of the density stratification on the triggering of both interface and free surface modes. We consider the same inclination of the plate ($\theta=0.2$) as in the studies of Loewenherz and Lawrence [2] and Chen [6], and assume zero interface and surface tensions ($S_1=S_2=0$).

In order to validate our code, we first plot the temporal growth rates of the interface mode for different Reynolds numbers in Fig. 2, similarly to what is shown in Figs. 7 and 13 of Chen [6] and with the same definitions of the growth rate and the Reynolds number. The agreement is so good that our curves could not be distinguished from Chen's curves. There is only one exception, for $U_1(1)\mathrm{Re}=2$, and we suspect a mistake in the plot of this curve in Chen's paper.

Chen [6] has shown that, for equal-density layers, inertia has a significant influence on the instability of the two-layer film flow. To see how this influence of inertia is modified by a density stratification effect, we select two situations corresponding to different depth and viscosity ratios, a first situation with $\delta=0.75$ and $m=2.5$ and a second situation with $\delta=1$ and $m=0.4$. In the first situation, the less viscous fluid is in the lower layer and in the second situation, it is in the upper layer. Both the interface and surface modes are considered. The neutral curves obtained in these different cases for different density ratios are plotted in Figs. 3 and 4.

The results for the interface mode are given in Fig. 3. In the first situation [less viscous layer adjacent to the wall; Fig. 3(a)], there are two separate unstable regions for $\gamma=1$ (equal-density layers) corresponding to a long- and a short-wave instability. These two instabilities exist at zero Reynolds number in agreement with the inertialess results of Loewenherz and Lawrence [2]. For $\gamma=1$, Chen [6] has shown that inertia stabilizes the long-wave instability (decrease of the growth rate) until it disappears above some critical value of Re, whereas it destabilizes the short-wave instability (increase of the growth rate). With decrease of the density ratio, it is found that the short-wave unstable region becomes smaller, until it disappears at a moderate Reynolds number when the density ratio is below a critical value, whereas the long-wave instability is favored as it occurs in a larger range

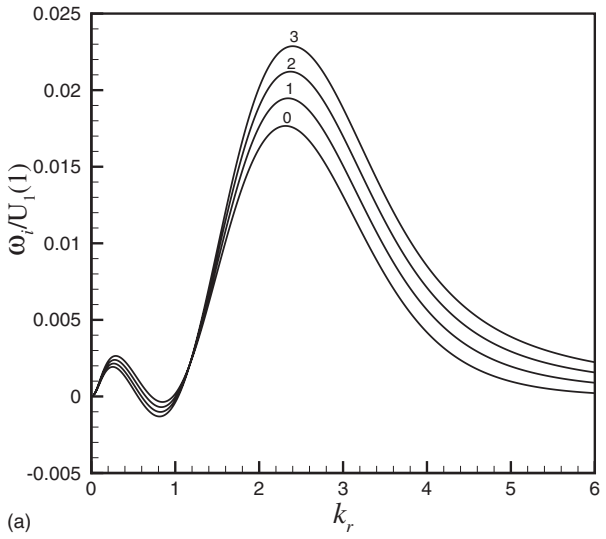

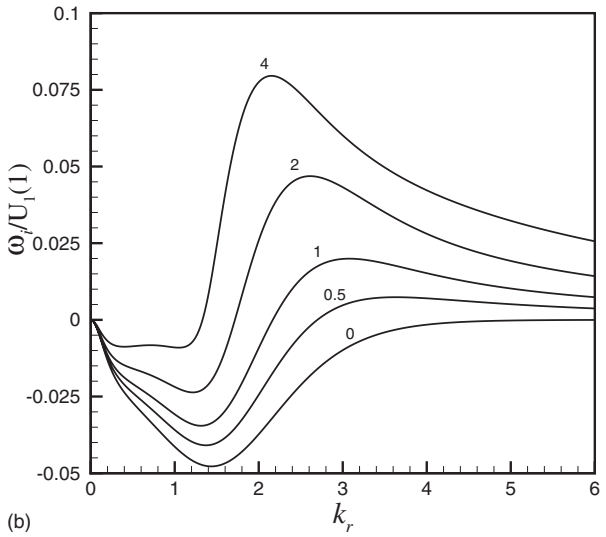

FIG. 2. Normalized temporal growth rates of the interface mode for different Reynolds numbers Re for (a) $\delta=0.75$, $m=2.5$ and (b) $\delta=1$, $m=0.4$. Above each curve, a figure indicates the corresponding value of $U_1(1)\mathrm{Re}$. The other parameters are $\gamma=1$, $S_1=S_2=0$, and $\theta=0.2$.

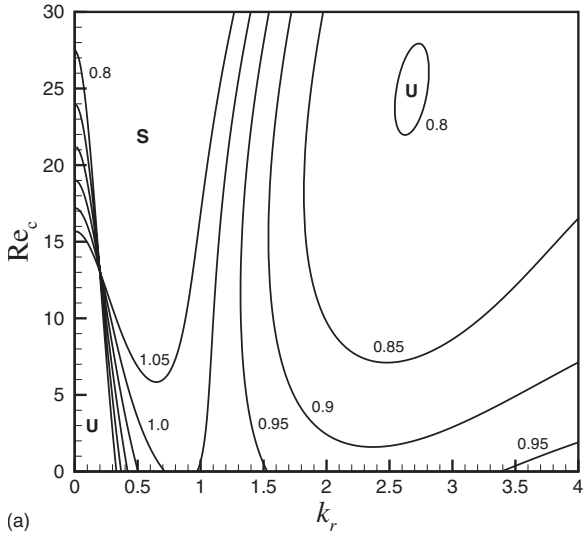

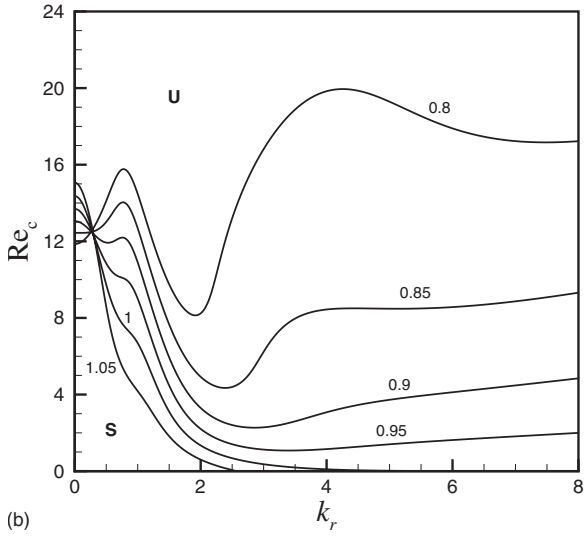

FIG. 3. Neutral curves of the interface mode for different density ratios γ in the Re-k_r plane for (a) $\delta=0.75$, $m=2.5$ and (b) $\delta=1$, $m=0.4$. For each neutral curve the corresponding density ratio is indicated. Note that the neutral curve for $\gamma=1$ approaches $\mathrm{Re}=0$ when $k_r\to\infty$ and thus never cuts the $\mathrm{Re}=0$ axis. The other parameters are $S_1=S_2=0$ and $\theta=0.2$.

of Reynolds number values. With the increase of the density ratio, the two long-wave and short-wave instability regions are found to rapidly connect.

In the second situation [more viscous layer adjacent to the wall; Fig. 3(b)], the unstable long- and short-wave regions are connected. For $\gamma=1$, Chen [6] has already shown that inertia destabilizes both long and short waves, and that the neutral curve delimits a stable region near the origin in the Re-k_r plane and then approaches $\mathrm{Re}=0$ when $k_r\to\infty$, indicating that the flow is linearly stable for $\mathrm{Re}=0$. This fact was confirmed in the inertialess study of Hu *et al.* [7]. Our results show that the decrease of the density ratio globally decreases the size of the unstable region with, in particular, a strong increase of the critical Reynolds number for the short-wave instability. For the long-wave instability, however, the critical Reynolds number above which the instability occurs decreases when γ is decreased. If we now focus on the region with small inertia, we see that, compared to the case $\gamma=1$ for which the neutral curve decreases asymptotically to $\mathrm{Re}=0$ as k_r is increased, for $\gamma=0.95$ there exists a nonzero critical Reynolds number below which the flow is linearly stable, for any value of k_r, whereas for $\gamma=1.05$ the neutral curve intersects the $\mathrm{Re}=0$ axis. These results indicate that, when the density ratio is above 1, a short-wave instability exists without the need for the destabilization by inertia. On the contrary, when the density ratio is below 1, inertia is necessary to trigger the short-wave interfacial instability. Finally, from the results shown in Figs. 3(a) and 3(b), we can conclude that it is not possible to stabilize both the short- and the long-wave interfacial instability simultaneously by changing the density ratio. Nevertheless, the use of density ratios smaller than 1 allows one to obtain Re regions where the two-layer

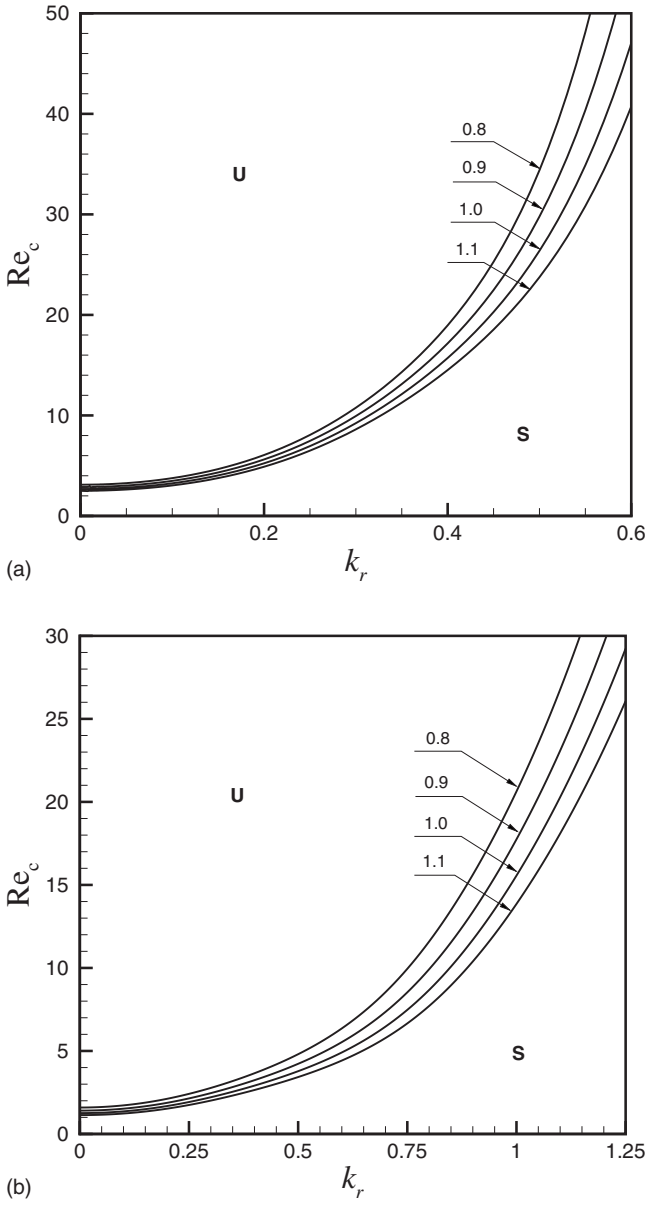

FIG. 4. Neutral curves of the surface mode for different density ratios γ in the Re-k_r plane for (a) $\delta=0.75$, $m=2.5$ and (b) $\delta=1$, $m=0.4$. For each neutral curve the corresponding density ratio is indicated. The other parameters are $S_1=S_2=0$ and $\theta=0.2$.

flow is stable with respect to the interface mode for all wavelengths: for $m=2.5$ (less viscous layer adjacent to the wall), this region is located above a critical Reynolds number, whereas for $m=0.4$ (more viscous layer adjacent to the wall), it is located below a critical Reynolds number.

The results for the surface mode are given in Fig. 4. In both situations $\delta=0.75$ and $m=2.5$ [Fig. 4(a)] and $\delta=1$ and $m=0.4$ [Fig. 4(b)], the instability is triggered above a critical Reynolds number which increases with k_r, and the decrease of the density ratio leads to the increase of this critical Reynolds number, indicating that more inertia is needed to trigger the surface mode instability. Nevertheless, the influence of the density ratio on the thresholds of the surface mode instability is rather weak, particularly in the long-wave region which is the more unstable.

IV. SPATIOTEMPORAL INSTABILITY

Basically, when an amplifying wave packet is convected away from its local position, the wave packet would be said to be convectively unstable [18–21]. If otherwise the amplification can be observed locally, the wave packet would be said to be absolutely unstable. Generally, the absolute or convective nature of the instability is determined by the sign of the absolute growth rate $\omega_{0i}=\mathrm{Im}[\omega(k_0)]$ defined at the saddle point k_0 of the dispersion relation, i.e., when $d\omega/dk|_{k_0}=0$. In these expressions, k is a complex wave number and ω is a complex frequency. If the absolute growth rate ω_{0i} is greater than zero (lower than zero), the flow is said to be absolutely (convectively) unstable. But it should be noticed that the saddle point k_0 used to identify the AI/CI must satisfy the Briggs-Bers collision criterion, i.e., the saddle point must be a pinch point produced by two distinct spatial branches of solutions of the dispersion relation $k_n^{\pm}(\omega)$, coming, respectively, from the upper and lower half k planes, and commonly referred to as upstream and downstream branches.

In order to clearly investigate the characteristics of the absolutely or convectively unstable two-layer flow, it is necessary to study the response of the flow to a localized disturbance along an arbitrary fixed spatiotemporal ray, $V=x/t$, as $t\to\infty$. This is equivalent to analyzing how the response evolves in a reference frame moving at the velocity V. If we introduce the Doppler-shifted frequency $\omega^v=\omega-Vk$ and use $k^v=k$, the dispersion relation in the moving coordinate system will be

$$D_v(k^v,\omega^v)=D(k^v,\omega^v+Vk^v)=0. \tag{11}$$

Because $d\omega^v/dk^v=0$, the saddle point $\tilde{k}$ will take place at

$$D(\tilde{k},\tilde{\omega})=0 \quad \text{and} \quad \frac{d\omega}{dk}(\tilde{k},\tilde{\omega})=V, \tag{12}$$

and then the absolute growth rate in the moving frame is obtained at $k_0^v=\tilde{k}$ through

$$\omega_0^v=\tilde{\omega}-V\tilde{k}. \tag{13}$$

Here also, the saddle point $\tilde{k}$ obtained from (12) must satisfy the Briggs-Bers collision criterion mentioned above. Obviously, the local growth rate for $V=0$ is just the absolute growth rate.

Still for the same inclination of the plate ($\theta=0.2$), we will consider the case where the less viscous layer is adjacent to the wall ($m=2.5>1$, $\delta=0.75$). In this case, we have seen in the previous section that the surface mode instability occurs above a critical Reynolds number whereas the interface mode instability occurs below a critical Reynolds number in the long-wave region and is observable in the finite-wave region for large enough density ratios. In order to study the spatiotemporal properties of these instabilities, we choose a moderate value of the Reynolds number, $\mathrm{Re}=8$, for which all these instabilities are effective. Our study will mainly focus on the density stratification effect.

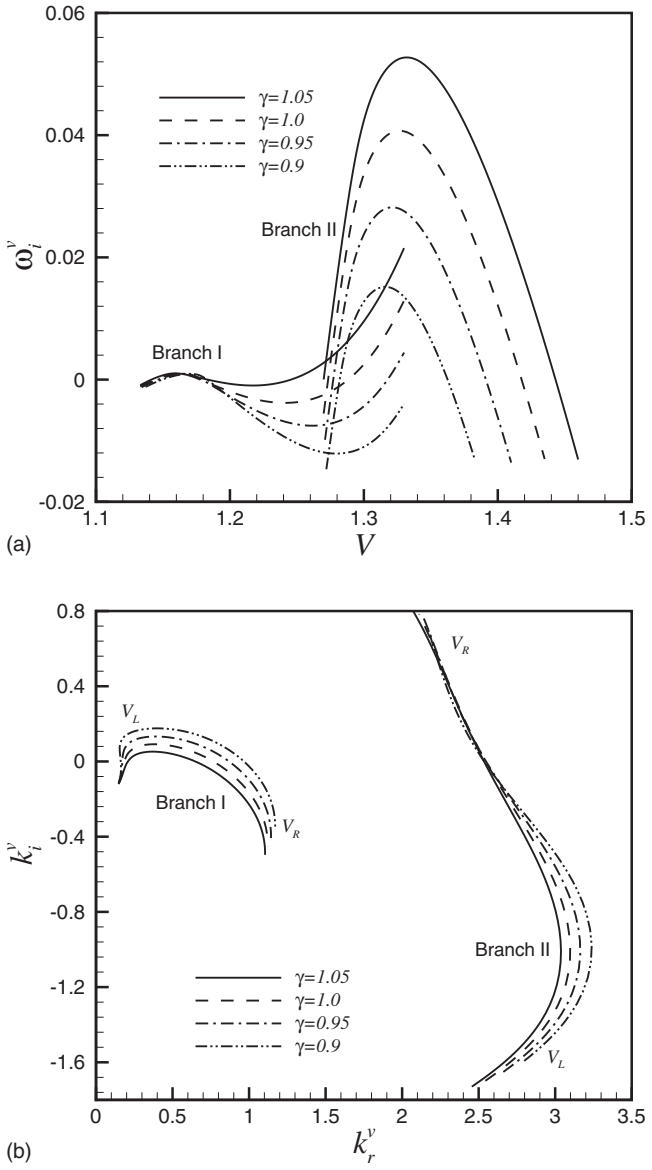

FIG. 5. Growth rate ω_i^v of the interface mode as a function of the ray velocity V for different density ratios γ (a) and corresponding loci of the saddle points in the complex k plane (b). In (b), V_R and V_L refer to the right and left boundaries of the unstable ray domains. The other parameters are Re=8, δ=0.75, m=2.5, S_1=S_2=0, and θ=0.2.

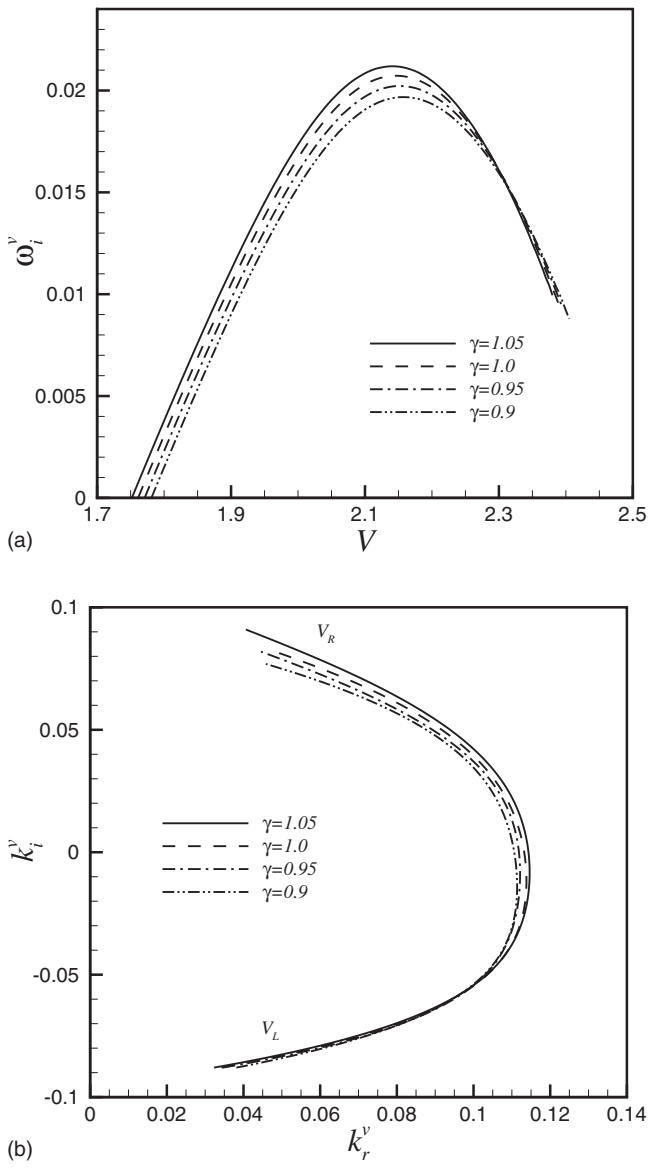

FIG. 6. Growth rate ω_i^v of the surface mode as a function of the ray velocity V for different density ratios γ (a) and corresponding loci of the saddle points in the complex k plane (b). In (b), V_R and V_L refer to the right and left boundaries of the unstable ray domains. The other parameters are Re=8, δ=0.75, m=2.5, S_1=S_2=0, and θ=0.2.

For the interface mode (Fig. 5) as well as the surface mode (Fig. 6), we give the growth rates ω_i^v as functions of the ray velocity V and the corresponding loci of the saddle points in the complex k plane. Our results are obtained by first finding all kinds of saddle points for an arbitrary ray velocity (such as V=1.3 for the interface mode), then using continuation to find the branches of those saddle points when V is varied by an iteration method (Deissler [22]; Yin *et al.* [23]).

For the interface mode (Fig. 5), it is shown that there exist two unstable branches of saddle points. These two unstable branches occur entirely for strictly positive values of the spatiotemporal ray velocity ($V>0$). The absolute growth rate in the laboratory frame (given by the local growth rate at V=0) is thus negative, indicating that the interfacial instability is convective for the chosen parameters. The branch in the left-hand side of the graphs corresponds to the long-wave instability (let us denote it "branch I"); the other branch corresponds to the short-wave instability and will be referred to as "branch II." The short-wave instability has the faster downstream velocity, and its maximum growth rate occurs near V=1.32. The long-wave instability has a slower downstream velocity. When the density ratio is 1.05, branch II has a much larger growth rate than branch I. But with the decrease of the density ratio, the growth rate of branch I, although small, remains almost constant in the domain around V=1.16, whereas the growth rate of branch II decreases

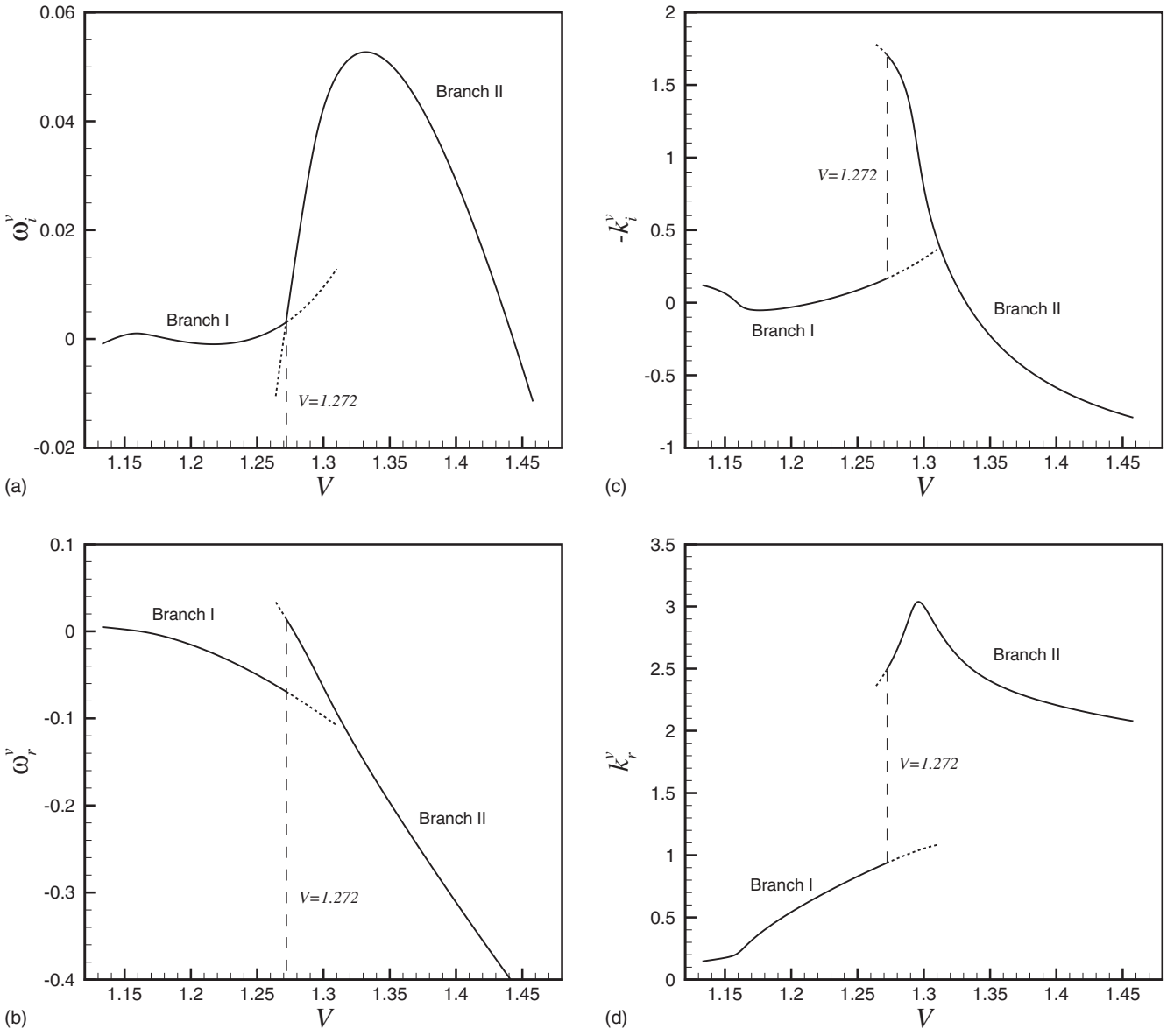

FIG. 7. (a) Growth rate ω_i^v, (b) oscillatory frequency ω_r^v, (c) local spatial amplification rate $-k_i^v$, and (d) local spatial wave number k_r^v as functions of the ray velocity V for $\gamma=1.05$. The other parameters are Re=8, $\delta=0.75$, $m=2.5$, $S_1=S_2=0$, and $\theta=0.2$.

quickly, in agreement with the suppression of the short-wave instability observed for smaller density ratios in Sec. III. Furthermore, it is found that for $\gamma \geq 1.05$ the two branches intersect at a certain ray velocity with a positive growth rate. A transition between long- and short-wave instabilities can thus be expected at this intersection point. To confirm this transition, it is necessary to determine which one of these two modes is the dominant mode of interfacial instability in the vicinity of this point; this can also be done by using the Briggs-Bers collision criterion.

We choose to study this transition for $\gamma=1.05$. More information about this case is given in Fig. 7 through the plots of the growth rate ω_i^v, the oscillatory frequency ω_r^v, the local spatial amplification rate $-k_i^v$, and the local spatial wave number k_r^v as a function of the ray velocity V. We see that the intersection point is located at $V=1.272$ and that the evolution of the characteristics is clearly different for the two branches. For $\gamma=1.05$, we thus perform the same two pinching processes as in the papers of Brevdo *et al.* [13] and Hu *et al.* [7], for $V=1.27$ and 1.274, slightly below and above the value of V at the intersection point (Figs. 8 and 9). For $V=1.27$ (Fig. 8), it is found that a Briggs-Bers collision occurs at small wave number $[k^{\mathrm{I}}=(0.93,-0.15)]$ when the growth rate is decreased from $\omega_i=0.004$ to $\omega_i=0.002\,76$. Then, when the growth rate is decreased from $\omega_i=0.002\,76$ to $\omega_i=2.5\times10^{-5}$, another collision occurs, but now the saddle point (found at a larger wave number k^{II}) does not satisfy the Briggs-Bers collision criterion. From these collision analyses, we can conclude that branch I dominates the spatiotemporal growth when $V<1.272$, i.e., when the moving frame velocity is smaller than that of the intersection point. For $V=1.274$ (Fig. 9), through a similar analysis, it is found that a Briggs-Bers collision occurs at finite wave number $[k^{\mathrm{II}}=(2.53,-1.69)]$, while a non-Briggs-Bers collision

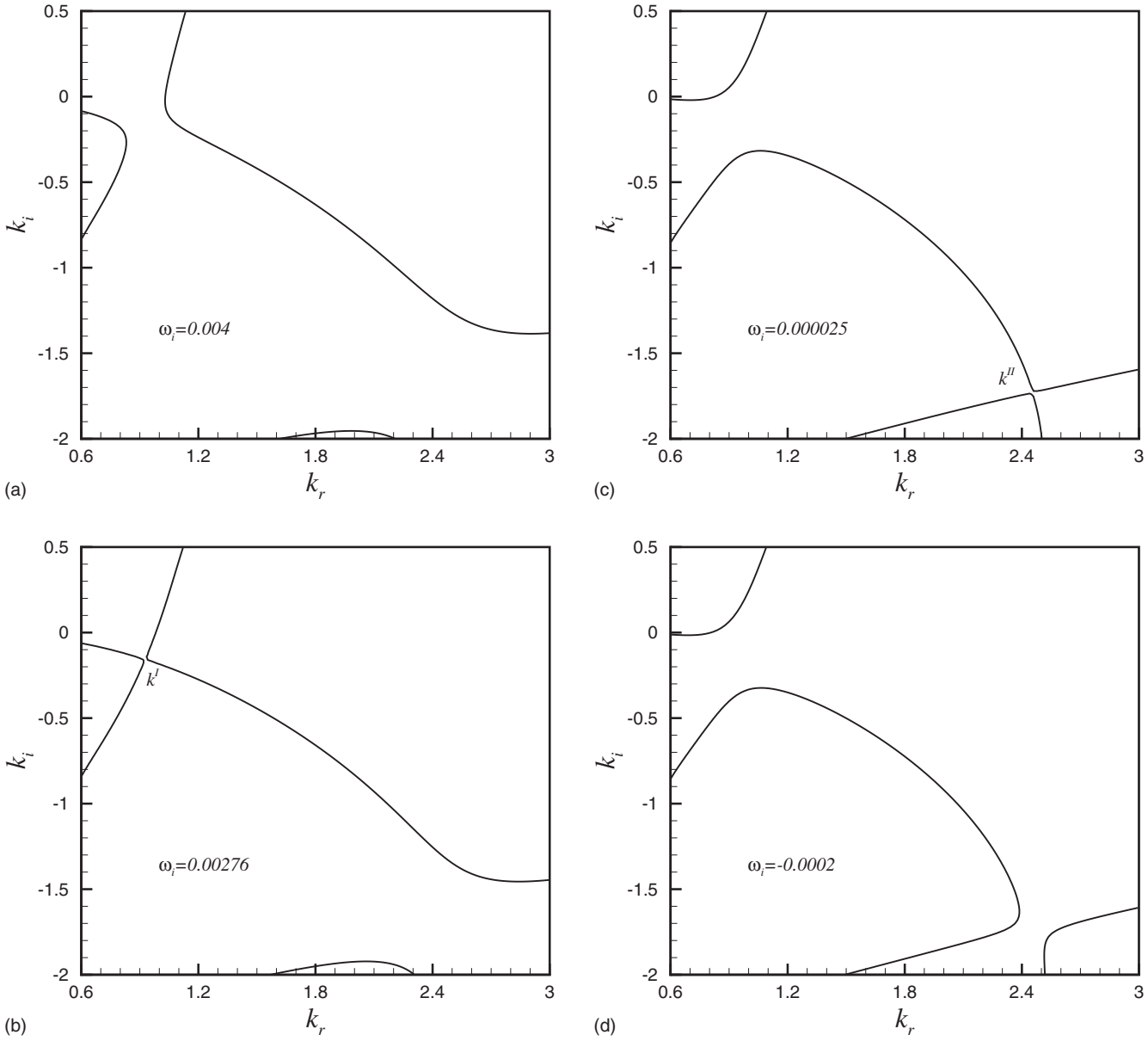

FIG. 8. Pinching process in the complex wave number plane (k_r, k_i) when the growth rate ω_i is decreased for $V=1.27$ and $\gamma=1.05$. The other parameters are Re=8, $\delta=0.75$, $m=2.5$, $S_1=S_2=0$, and $\theta=0.2$.

occurs at small wave number $[k^{\mathrm{I}}=(0.95,-0.17)]$, which shows that the spatiotemporal growth is dominated by branch II when $V>1.272$. Considering Fig. 7(a), we can conclude that the Briggs-Bers collision criterion is satisfied at the saddle points corresponding to the parts of the branches which have the larger growth rate. The intersection point at $V=1.272$ is then a real transition point which can be used to distinguish the long- and short-wave instabilities for the interface mode of the two-layer film flow. Furthermore, as can be seen clearly in Figs. 7(b)–7(d), the oscillatory frequency, local spatial amplification rate, and local spatial wave number are found to jump from branch I to branch II at this transition point, which indicates a discontinuity for these quantities.

For the surface mode (Fig. 6), it is shown that there exists only one unstable branch of saddle points. This branch corresponds to a surface wave instability which has a larger downstream velocity than the interfacial wave instabilities, and is thus also convective. The wavelengths of this surface instability are also much larger than those obtained for both branch I and branch II of the interfacial instability. With the decrease of the density ratio, the surface wave instability has smaller growth rates. Nevertheless, from the results of Sec. III, we cannot expect that a small density ratio will completely suppress the surface wave instability.

V. ABSOLUTE TO CONVECTIVE INSTABILITY TRANSITION

Due to the presence of the absolute Rayleigh-Taylor instability for $\theta=0$, it can be expected that the instability due to the interface will become absolutely unstable when the in-

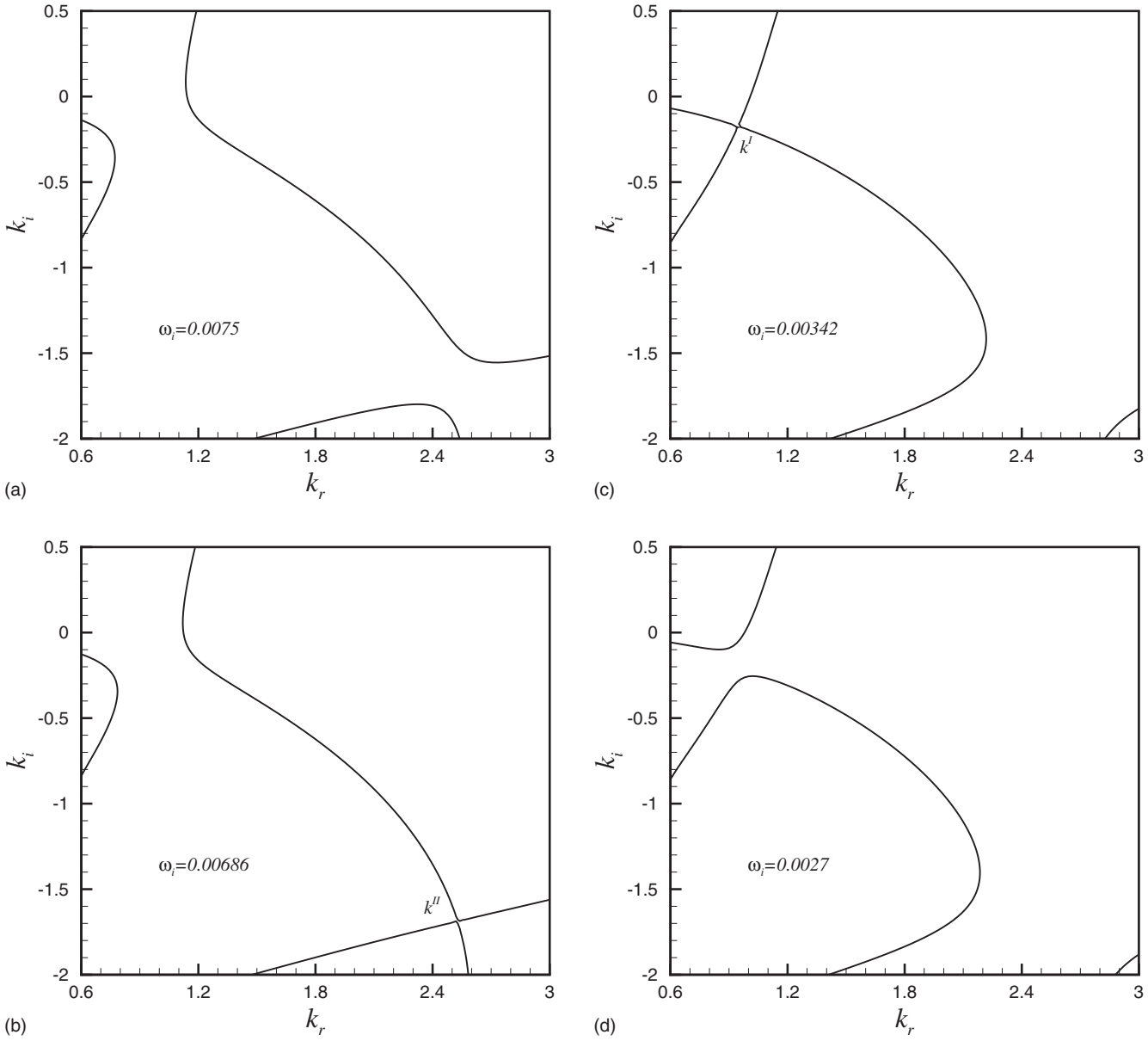

FIG. 9. Pinching process in the complex wave number plane (k_r, k_i) when the growth rate ω_i is decreased for $V=1.274$ and $\gamma=1.05$. The other parameters are Re=8, $\delta=0.75$, $m=2.5$, $S_1=S_2=0$, and $\theta=0.2$.

cline angle approaches zero and the upper layer has the higher density ($\gamma>1$). This transition from convective to absolute instability has already been detected by Hu *et al.* [7] in his inertialess stability study of the two-layer film flow. Here, we consider this transition in the more practical situation where the inertia effect is taken into account. The results are shown in Fig. 10 where the boundary curves between absolute and convective instability are plotted for different values of the parameters.

We first consider a fixed value of the plate inclination, $\theta=0.02$, and give the boundary curves in the δ-γ plane for different values of Re and $m=2.5$ [Fig. 10(a)] and in the Re-γ plane for different values of m and $\delta=0.75$ [Fig. 10(b)]. From Fig. 10(a), we see that there is a minimum for the critical density ratio and that this minimum occurs at a moderate depth ratio. With the increase of the Reynolds number ($0\leq \mathrm{Re}\leq 3$), the minimum critical density ratio increases and the absolutely unstable region decreases in size, indicating that it is more difficult to make the two-layer system absolutely unstable. The depth ratio δ at the minimum of γ also depends on Re and evolves from 1 to 0.75 when Re is changed from 0 to 3. More details on the influence of Re are given in Fig. 10(b) for a fixed depth ratio $\delta=0.75$. From this figure, we see that the absolutely unstable region finally disappears above a limit Reynolds number, indicating thus that the flow can only be convectively unstable beyond this limit value of Re. This limit value is rather small (Re around 4 for $m=2.5$) and varies a little with the viscosity ratio m. The general influence of m on the boundary curves is also depicted in Fig. 10(b): the main effect is that, for small Reynolds numbers, the decrease of the viscosity ratio will allow

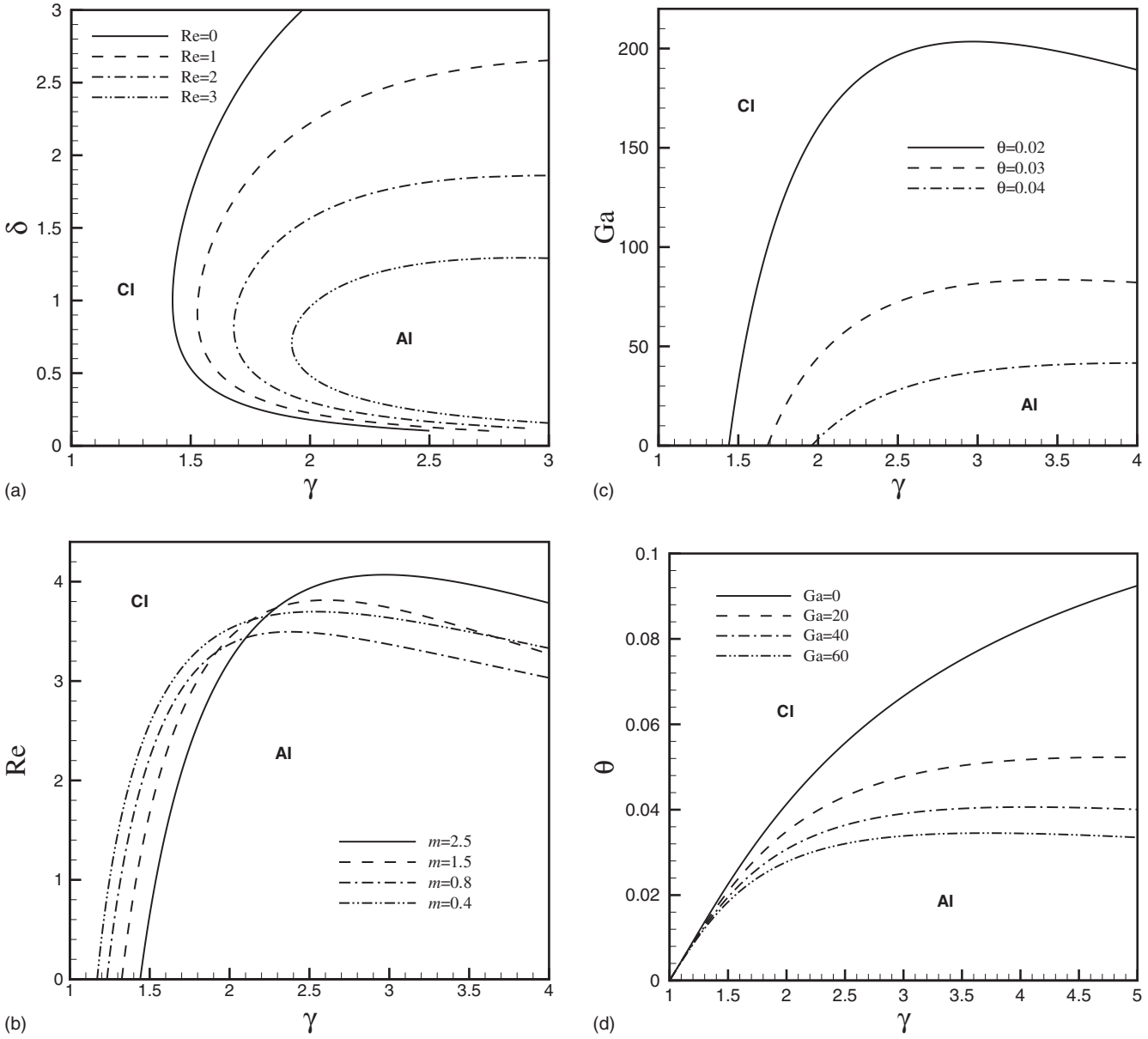

FIG. 10. Boundary curves between absolute and convective instability: (a) δ-γ curves for $\theta=0.02$, $m=2.5$, and different Reynolds numbers Re, (b) Re-γ curves for $\theta=0.02$, $\delta=0.75$, and different viscosity ratios m, (c) Ga-γ curves for $m=2.5$, $\delta=0.75$, and different incline angles θ, and (d) θ-γ curves for $m=2.5$, $\delta=0.75$, and different Galileo numbers Ga. The other parameters are $S_1=S_2=0$.

the flow to become absolutely unstable at a smaller density ratio.

The effect of the incline angle θ on the boundary curves is then presented in Figs. 10(c) and 10(d) for fixed viscosity ratio $m=2.5$ and fixed depth ratio $\delta=0.75$. As the Reynolds number Re contains θ [more precisely $\sin(\theta)$] in its definition [see Eqs. (3) and (1)], it is preferable to introduce the Galileo number $\mathrm{Ga}=\mathrm{Re}/\sin\theta$ to quantify the inertia effect when the incline angle is modified. Figure 10(c) depicts the boundary curves in the Ga-γ plane for different incline angles θ and Fig. 10(d) the boundary curves in the θ-γ plane for different Galileo numbers Ga. From Fig. 10(c), it can be seen that, at constant θ [similarly to what is found in Fig. 10(b) for $\theta=0.02$], there exists a limit Galileo number above which the flow can only be convectively unstable. With the increase of the incline angle, this limit value strongly decreases and the region of absolute instability is reduced toward smaller values of Ga and larger values of γ. Finally, Fig. 10(d) shows that, at fixed Galileo number, there also exists a limit incline angle above which the flow can only be convectively unstable. With the increase of the Galileo number, the limit incline angle decreases and this limit value is reached at a smaller density ratio. Note that, when the incline angle is decreased, the critical density ratio approaches 1 for all Galileo numbers, in agreement with the characteristics of the Rayleigh-Taylor instability which occurs at $\theta=0$.

VI. SPATIALLY AMPLIFYING WAVES

In the previous sections, we have learned that, in most of the parameter space, the two-layer film flow becomes un-

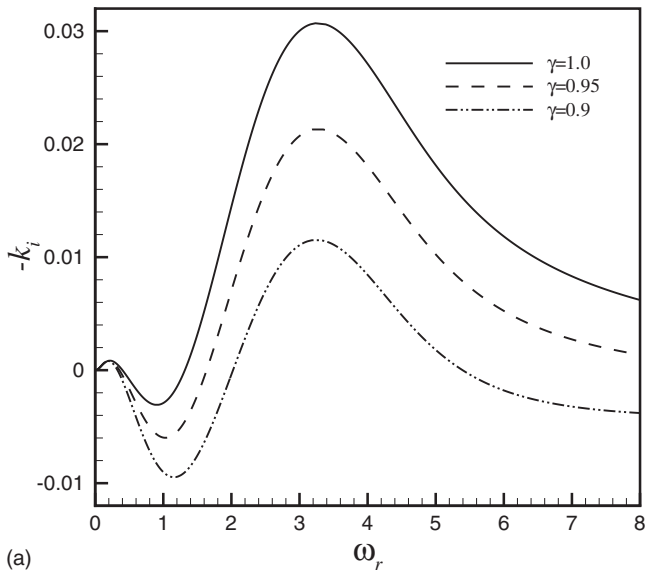

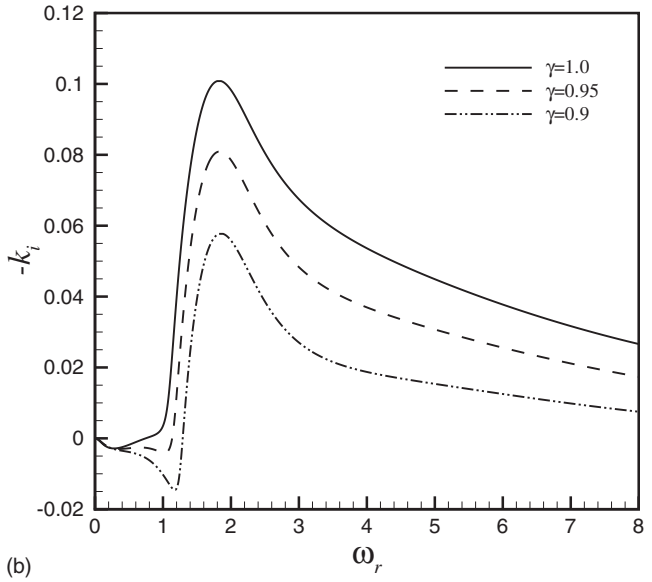

FIG. 11. Spatial growth rate $-k_i$ of the interface mode as a function of the forcing angular frequency ω_r for different density ratios γ: (a) $\delta=0.75$, $m=2.5$ and (b) $\delta=1$, $m=0.4$. The other parameters are Re=8, $S_1=S_2=0$, and $\theta=0.2$.

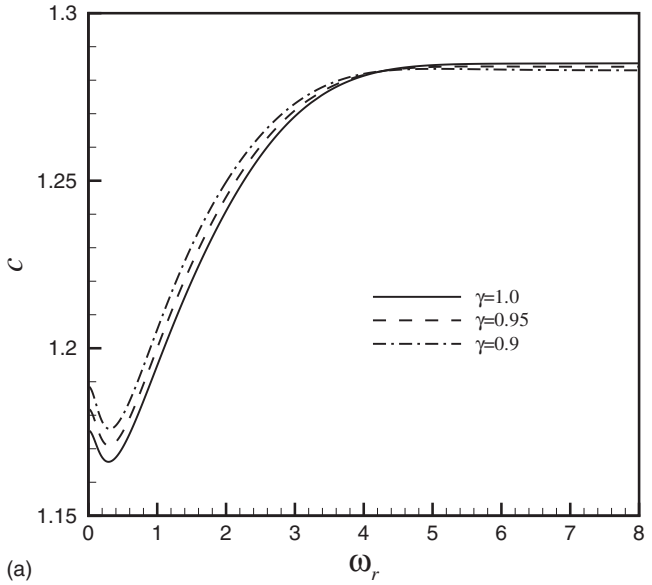

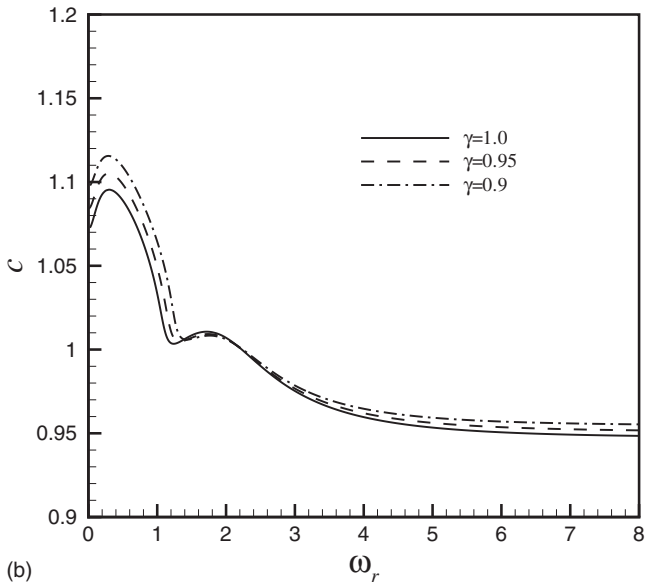

FIG. 12. Phase speed c of the interface mode as a function of the forcing angular frequency ω_r for different density ratios γ: (a) $\delta=0.75$, $m=2.5$ and (b) $\delta=1$, $m=0.4$. The other parameters are Re=8, $S_1=S_2=0$, and $\theta=0.2$.

stable only in a convective way, with the exception of a region at small incline angle and small inertia effect where absolute instability can occur. In a large region of the parameter space, the unstable perturbations in the two-layer film flow are thus convected downstream. To get more information on these convected waves, it is interesting to study the spatial amplification of the linear waves generated by a spatially localized harmonic forcing with small amplitude. In fact, the response to a periodic forcing, usually referred to as a signaling problem, is determined by a spatial instability analysis which can be formulated as

$$D(k,\omega_r)=0. \tag{14}$$

The spatial growth rates $-k_i$ and spatial wave numbers k_r are computed as functions of the forcing angular frequency ω_r by an iteration method. From the spatial wave number k_r, we can also calculate the phase speed $c=\omega_r/k_r$, which is a quantity easier to measure in experiments. As in Sec. III, we successively consider the interface mode and the surface mode, and for each mode select the same two situations ($\delta=0.75$, $m=2.5$ and $\delta=1$, $m=0.4$) for Re=8.

The results for the interface mode are first presented in Figs. 11 and 12. The variations of the spatial growth rates $-k_i$ with the forcing frequency ω_r for different density ratios are shown in Fig. 11. In the first situation [less viscous layer adjacent to the wall; Fig. 11(a)]), there exist both low frequency and high frequency spatially amplifying waves, whereas in the second situation (more viscous layer adjacent to the wall (Fig. 11(b)], there exist only high-frequency spa-

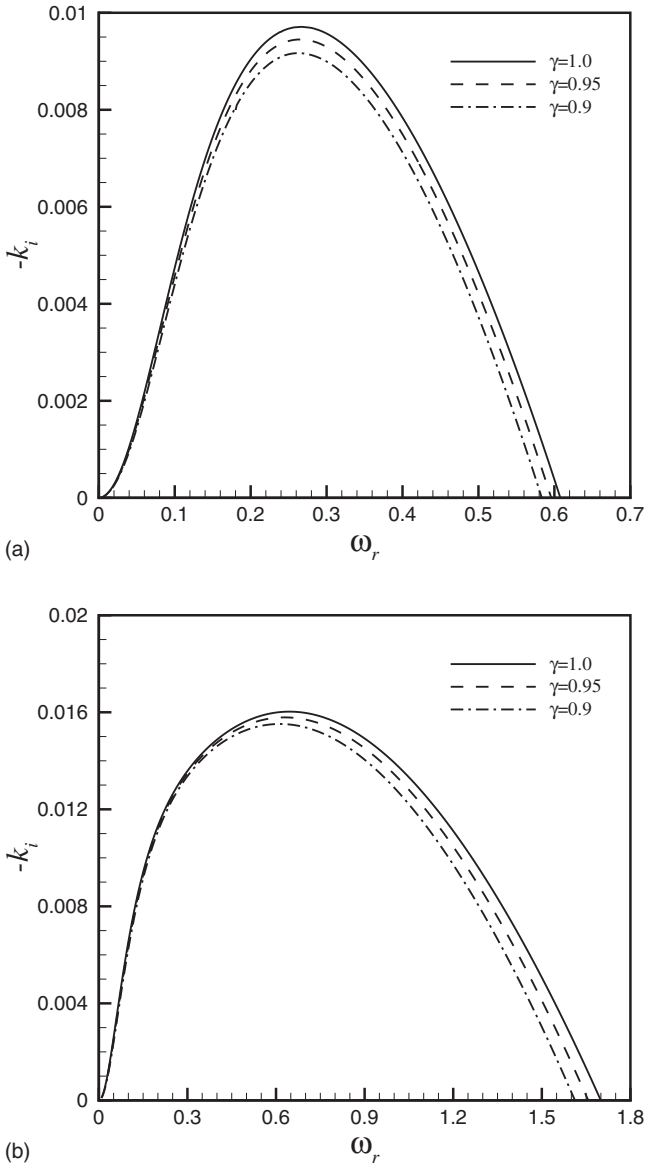

FIG. 13. Spatial growth rate $-k_i$ of the surface mode as a function of the forcing angular frequency ω_r for different density ratios γ: (a) $\delta=0.75$, $m=2.5$ and (b) $\delta=1$, $m=0.4$. The other parameters are Re=8, $S_1=S_2=0$, and $\theta=0.2$.

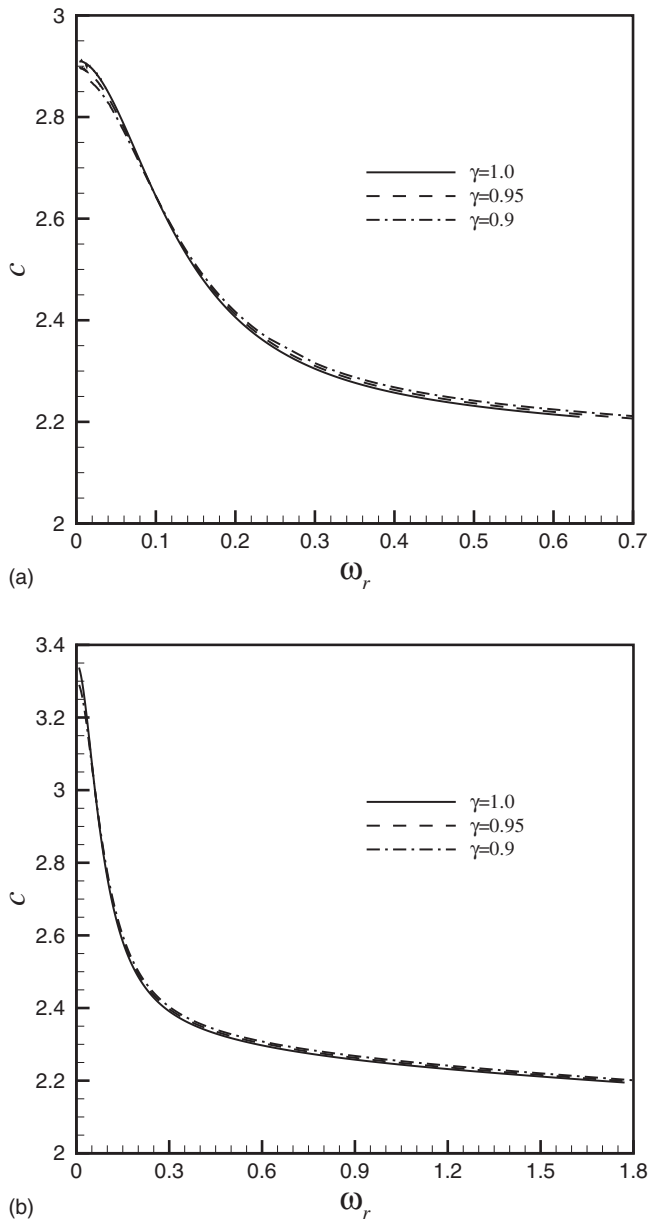

FIG. 14. Phase speed c of the surface mode as a function of the forcing angular frequency ω_r for different density ratios γ: (a) $\delta=0.75$, $m=2.5$ and (b) $\delta=1$, $m=0.4$. The other parameters are Re=8, $S_1=S_2=0$, and $\theta=0.2$.

tially amplifying waves, similar similarity to what is obtained in the temporal instability analysis (Sec. III) in terms of temporal growth rate. The decrease of the density ratio is found to decrease the spatial growth rate: this influence is weak for small forcing frequency, but particularly strong at the level of the peaks at moderate forcing frequency in connection with the evolutions of the temporal short-wave instability observed in Figs. 3(a) and 3(b). The phase speeds c of these spatial waves are then shown as a function of the forcing frequency ω_r in Fig. 12. In the first situation ($\delta=0.75$ and $m=2.5$), the phase speed presents a minimum at the level of the long-wave instability, then increases with the increase of ω_r in the region of the short-wave instability, and finally tends to a constant phase speed [Fig. 12(a)]. In the second situation ($\delta=1$ and $m=0.4$), in the region affected by the short-wave instability ($\omega_r>1.2$), we find a small increase of the phase speed toward a maximum at the level of the growth rate peak, before a clear decrease toward an asymptotic constant phase speed [Fig. 12(b)]. The phase speeds are somewhat smaller in the second situation. The influence of the density ratio on the phase speed is rather weak and not easy to characterize.

The evolutions of the spatial growth rates $-k_i$ and phase speeds c with the forcing phase frequency ω_r are then plotted for the surface mode in Figs. 13 and 14, respectively. It is found that both situations studied ($\delta=0.75$, $m=2.5$ and $\delta=1$, $m=0.4$) give the same type of evolution for $-k_i$ as well as for c. A single positive peak at small forcing frequency is

obtained for the spatial growth rate [Figs. 13(a) and 13(b)], indicating that the spatially amplifying waves are long waves. The peak intensity decreases with the decrease of the density ratio γ, but this influence is smaller than for the interface short-wave modes. The phase speed of these amplifying waves continuously decreases with the increase of ω_r, first quite quickly and then more slowly, and the influence of γ on this evolution is very small [Figs. 14(a) and 14(b)]. Finally, it is interesting to note that the phase speeds obtained for these long-wave surface modes are clearly stronger than those obtained for the interface modes.

VII. CONCLUSION

The temporal and spatiotemporal instabilities occurring in two-layer falling films have been investigated by using the Chebyshev collocation method to solve the full system of linear stability equations. The different effects involved (inertia, density and viscosity stratification, depth ratio, inclination of the plate) have been taken into account; only the stabilizing influence of interface and surface tensions has not been considered. The neutral curves $\mathrm{Re}(k)$ for both the surface mode and the interface mode of instability have been obtained by a temporal stability analysis. Long- and short-wave interfacial instabilities are detected, which also exist, as expected, for $\mathrm{Re}=0$ (inertialess instability), whereas a long-wave surface instability is found above a critical Reynolds number. The decrease of the density ratio always make the surface mode and the short-wave interface mode more stable; it can even make the short-wave inertialess instability disappear. Moreover, when the less viscous layer is in the region next to the wall, a small enough density ratio can completely suppress the short-wave instability of the interface mode, so that there exist only long-wave instabilities of the surface mode and interface mode. On the contrary, the decrease of the density ratio favors the long-wave interfacial instability which exists in a larger range of Reynolds number values.

The spatiotemporal analysis shows that the instability is convective for incline angles that are not too small, like $\theta=0.2$. The study of the local growth rates of the spatiotemporal instability as a function of the ray velocity V shows that there is a transition between long- and short-wave convective instabilities. Accordingly, there exists a jump for the local oscillatory frequency, spatial amplification rate, and spatial wave number due to this transition.

Due to the existence of the absolute Rayleigh-Taylor instability for $\gamma>0$ and $\theta=0$, a transition from convective to absolute instability has been detected at small incline angles. From the absolute and convective instability boundary curves, it is found that there exist limit values of the Reynolds number (for a fixed small incline angle) and of the incline angle (for a fixed Galileo number) above which the two-layer film flow can only be convectively unstable.

Finally, a spatial instability analysis has been performed in order to characterize the spatial amplification of the linear waves in the convectively unstable region of the parameter space. The interface waves generated by a high-frequency forcing can have large growth rates, but these growth rates strongly diminish when the density ratio is decreased, so that these waves eventually die out for small enough density ratios. On the contrary, the interface or surface waves generated by a low-frequency forcing have smaller growth rates, but these growth rates are only slightly influenced by variations of the density ratio. Note finally that the surface waves have larger phase speeds than the interface waves.

ACKNOWLEDGMENTS

This work was funded by a program from the Région Rhône-Alpes (J.H.). This work was also supported by the National Natural Science Foundation of China (Grant Nos. 10676005, 10676004, 10676120, and 10702011).

[1] K. P. Chen, Appl. Mech. Rev. **48**, 763 (1995).
[2] D. S. Loewenherz and C. J. Lawrence, Phys. Fluids A **1**, 1686 (1989).
[3] T. W. Kao, Phys. Fluids **8**, 812 (1965).
[4] T. W. Kao, J. Fluid Mech. **33**, 561 (1968).
[5] C. S. Yih, Phys. Fluids **6**, 321 (1963).
[6] K. P. Chen, Phys. Fluids A **5**, 3038 (1993).
[7] J. Hu, S. Millet, V. Botton, H. B. Hadid, and D. Henry, Phys. Fluids **18**, 104101 (2006).
[8] W. Y. Jiang, B. Helenbrook, and S. P. Lin, Phys. Fluids **16**, 652 (2004).
[9] A. F. M. Akhtaruzzaman, C. K. Wang, and S. P. Lin J. Appl. Mech. **45**, 25 (1978).
[10] C. K. Wang, J. J. Seaborg, and S. P. Lin, Phys. Fluids **21**, 1669 (1978).
[11] S. J. Weinstein and M. R. Kurz, Phys. Fluids A **3**, 2680 (1991).
[12] S. J. Weinstein and K. P. Chen, Phys. Fluids **11**, 3270 (1999).
[13] L. Brevdo, P. Laure, F. Dias, and T. J. Bridges, J. Fluid Mech. **396**, 37 (1999).
[14] J. Liu and J. P. Gollub, Phys. Rev. Lett. **70**, 2289 (1993).
[15] J. Liu, J. D. Paul, and J. P. Gollub, J. Fluid Mech. **250**, 69 (1993).
[16] C. Canuto, M. Y. Hussaini, A. Quarteroni, and T. A. Zang, *Spectral Methods in Fluid Dynamics* (Springer-Verlag, New York, 1988).
[17] D. A. Goussis and A. J. Pearlstein, J. Comput. Phys. **84**, 242 (1989).
[18] R. J. Briggs, *Electron-Stream Interaction with Plasmas* (MIT Press, Cambridge, MA, 1964).
[19] A. Bers, in *Survey Lectures, Proceedings of the International Congress on Waves and Instabilities in Plasmas*, edited by G. Auer and F. Cap (Institute for Theoretical Physics, Innsbruck, 1973, p. B1.
[20] P. Huerre and P. A. Monkewitz, J. Fluid Mech. **159**, 151 (1985).
[21] P. Huerre and P. A. Monkewitz, Annu. Rev. Fluid Mech. **22**, 473 (1990).
[22] R. J. Deissler, Physica D **25**, 233 (1987).
[23] X. Y. Yin, D. J. Sun, M. J. Wei, and J. Z. Wu, Phys. Fluids **12**, 1062 (2000).